Astron. Astrophys. 357, 743–756 (2000)

ASTRONOMY AND ASTROPHYSICS

SUMER observations of transition region fine structures

E. Landi[1,2], **H.E. Mason**[3], **P. Lemaire**[4], **and M. Landini**[2]

[1] Max-Planck-Institut für Aeronomie, 37191 Katlenburg-Lindau, Germany
[2] Dipartimento di Astronomia e Scienza dello Spazio, Università di Firenze, Italia
[3] Department of Applied Mathematics and Theoretical Physics, Silver Street, Cambridge CB3 9EW, UK
[4] Institut d'Astrophysique Spatiale, Unité Mixte CNRS – Université de Paris XI, Bat 121, 91405 Orsay, France

Received 16 November 1999 / Accepted 24 March 2000

Abstract. The SUMER (Solar Ultraviolet Measurements of Emitted Radiation) instrument on SOHO (Solar and Heliospheric Observatory) provides an opportunity to observe and study the solar transition region with high spatial and spectral resolution. We present new evidence to confirm that the emission from the quiet Sun at 2×10^5 K is dominated by cool loop-like fine structures which cluster across the chromospheric network boundaries. The electron density of these structures is found to be around 10^{10} cm^{-3}. The red-shifts in spectral line profiles and the non-thermal widths from lines formed at this temperature are found to be correlated with intensity. The properties of explosive events with irregular profiles are explored. A large jet-like structure is analysed. The results of our analysis are compared with recent predictions from numerical models.

Key words: Sun: corona – Sun: transition region – Sun: UV radiation

1. Introduction

A seminal paper by Gabriel (1976) provided a model for the solar atmosphere which took account of the magnetic field geometry resulting from supergranular convective flux. This model has become a benchmark for theoretical models of the temperature and density structure in the quiet Sun. Recently, Gallagher et al. (1999) have studied quiet Sun observations obtained with the Coronal Diagnostic Spectrometer (CDS, Harrison et al. 1995) and find that they broadly support the model of Gabriel (1976). A heated debate has been raging on the nature of the transition region, at a temperature of around 10^5 K, which separates the chromosphere and corona. Early models (cf Gabriel & Mason, 1982) were based on a plane parallel atmosphere and are no longer appropriate to describe the dynamic and inhomogeneous nature of the transition region.

Analyses of Skylab observations led to the proposal by Feldman (1983) that the transition region is composed of Unresolved Fine Structures (UFSs). Feldman & Laming (1994) provided evidence to suggest that most of the low temperature transition region ($< 7 \times 10^5$ K) and the coronal emission ($> 10^6$ K) is disconnected, that is not part of continuous atmospheric structures.

Observations of the transition region in UV emission from instruments such as the High Resolution Telescope and Spectrometer (HRTS) (Brueckner & Bartoe, 1983) showed inhomogeneities on a scale at the spatial resolution of the instrument (1"). The electron density values derived from the O IV emission lines indicated the existence of sub-resolution filamentary structures, with fill factors of $10^{-2} - 10^{-5}$ (Dere et al., 1987). Dere and co-authors concluded that the macroscopic structures seen in C IV emission were probably composed of discrete, sub-resolution structures.

Antiochos & Noci (1986) proposed the co-existence of hot and cool loops to explain a different puzzle, the upturn in the emission measure towards the lower temperatures. Dowdy et al. (1986) went one step further to describe the transition region as a *magnetic junkyard*, comprising cool loops (around 10^5 K) of varying sizes and hotter (around 10^6 K) large loops or *funnels*.

Wikstol et al. (1998) re-examined the evidence for UFSs, which are magnetically and thermally disconnected from the corona, and the Classical Transition Region (CTR) models which provide continuity between the cool and hot plasma. They were very critical of the empirical approach adopted by Feldman and co-workers and suggest that a forward approach to modelling the solar atmosphere should be adopted. They stressed the non-uniqueness of inferring physical plasma properties from observations. In particular, they were concerned that plasma processes in the solar atmosphere are dynamic and time-dependent.

Recently, Feldman et al. (1999) have re-examined the observational evidence for the morphology of the quiet solar upper atmosphere. They review data from the Skylab S082a spectroheliograph, the Transition Region and Coronal Explorer (TRACE), YOHKOH and SOHO. The coronal emission (T between 10^6 K and 2×10^6 K) in the quiet Sun clearly originates from a large number of densely packed loop-like structures. From SUMER and Skylab observations, Feldman et al. confirm that at lower temperatures ($< 8 \times 10^5$ K) the emission originates predominantly in cool loop-like structures, which are brightest along the chromospheric network.

Spectral line shifts and broadenings provide a diagnostic tool for probing the dynamics of the solar atmosphere. System-

Send offprint requests to: E.Landi (enricol@arcetri.astro.it)

atic redshifts in transition region lines have been observed in both solar and stellar spectra. A persistent redshift is observed in the quiet Sun transition region lines. Brekke et al. (1997), Chae et al. (1998b), Peter (1999) give useful summaries of recent observations with SUMER. Several authors have studied the spectral line broadening of transition region and coronal emission from Skylab, HRTS and more recently SUMER. The non-thermal broadening can provide a useful constraint on the possible heating mechanisms for the solar plasma (Doyle et al., 1997, Erdelyi et al., 1998a). The correlation between the line profile and redshift for active and quiet regions is discussed by Brynildsen et al. (1998) and Teriaca et al. (1999a).

The HRTS observations of C IV emission showed a dynamic transition region with a multitude of explosive events (Brueckner & Bartoe, 1983, Dere et al., 1989, Dere, 1994). The average extent of these explosive events was found to be 1500 km, with Doppler shifts giving typical maximum velocities of 150 km s^{-1} in both the blue and red wings, with an average lifetime of 60 s. Innes et al. (1997) reported the observation of similar bi-directional jets in Si IV using SUMER. Chae et al. (1998a) found a strong tendancy for explosive events to occur repeatedly in bursts. These could be sites of magnetic energy release. Small scale brightenings have also been observed with CDS (*blinkers*, Harrison, 1997, Harrison et al., 1999) and EIT (Berghmans et al., 1998). All these events seem to be located at or near the network boundaries and could be related to the nano-flare activity proposed by Parker (1998). Krucker & Benz (1998) and Benz & Krucker (1999), using data from SOHO and radio observations, have shown that intensity variations in chromospheric/transition region emission in small scale brightenings correlate with coronal variations in the same way as in solar flares. They also show that such events, if interpreted as microflares and nanoflares, can be responsible at least for a substantial part of heating in quiet solar corona.

In this paper we re-examine the nature of the transition region using the impressive spatial and spectral capability of the SUMER instrument on SOHO. Preliminary results were presented at the SOHO 7 workshop in September, 1998 (Landi et al., 1999a). In Sect. 2 we describe the SUMER instrument, observations and data reduction. In Sect. 3 we present intensity maps of transition region, coronal and chromospheric lines over a large spatial area. In Sect. 4 we analyse the spectral line shifts, widths and the electron density and temperature distribution for the quiet features. In Sect. 5, we discuss the more active features, explosive events, which have broader line profiles, together with a jet-like structure. In Sect. 6, we summarise our results and the implications which these have for transition region models.

2. Observations and data reduction

The SUMER spectrometer on SOHO is able to make extreme- to far-ultraviolet spectral observations within the 465 to 1610 Å range, with a pixel size between 0.042 and 0.044 Å (in the grating first order) and a spectral resolving power between 17700 and 38300. Simultaneous windows can be selected within the 1024 spectral pixels (43 to 45 Å, in first order) of the detector.

Table 1. Details of SUMER observations on Sept. 16–17, 1996 (* and ** indicate the grating first and second order).

Parameters	SEP16 (1996)	SEP17 (1996)
Observation time (UT)	16:01–22:54	3:30–6:52
Slit (arcsec^2)	1×300	1×120
Raster step (arcsec)	0.76	0.76
Effective step (arcsec)	0.59	0.47
Raster size (arcsec)	236	47
Field of view (arcsec^2)	236×300	47×120
Exposure time (second)	60	105
Window width (Å)	2.2	2.2
Wavelength range	Observed ions	
1240–43,1237–40	N V*	
623.9–626.0	Mg X**	
628.6–630	O V**	
	Si I*, Si II*	
1384–1428		Si IV*,O IV*
		S IV*,O III**

Several entrance slits can be selected (from 0.3 x 120 arcsec^2 to 4 x 300 arcsec^2) and the solar image can be scanned with a step size, which is any multiple of 0.38 arcsec (see Wilhelm et al., 1995, 1997 and Lemaire et al., 1997). The two datasets analyzed in the present study were observed on 1996 September 16 and 17 (SEP16 and SEP17 respectively). They consist of two large quiet Sun rasters at disk centre corresponding to different grating positions. Each raster is built by steps of 0.76 arcsec on the solar image using a one arcsecond slit width. Details are given in Table 1.

The SEP16 dataset is the spectrum of a solar quiet region 236×300 arcsec^2 with four spectral windows selected in order to include some strong transition region lines (N V and O V) together with a coronal line (Mg X). Wavelength ranges and spectral lines are given in Table 1. During the 60 second exposure time the Sun rotated by ≈ 0.17 arcsec, so the effective raster step was 0.59 arcsec. The total observing time was 6h 46m.

SEP17 dataset consists of the spectrum of a solar quiet region 47×110 arcsec^2 in the 1384–1428 Å spectral range, with 105 s exposure time and 0.47 arcsec effective raster step. This dataset includes a strong Si IV line and an O IV multiplet which provides density diagnostics for the transition region at around 10^5 K. The total observing time was 3h 15m.

Data reduction was carried out using standard routines allowing flat-field and radiometric calibration. Calibrated data units are phot cm^{-2} s^{-1} sr^{-1} Å^{-1}. Data have been corrected for distortions in the image formed on the detector.

3. Structure of the transition region

The large spatial area covered by these observations together with the good count rates provide an excellent opportunity to study the overall nature and structure of the transition region, in relationship to the underlying network structure. It is well known that the transition region is dynamic, so these observations simply provide a snapshot of the general features. Gaussian

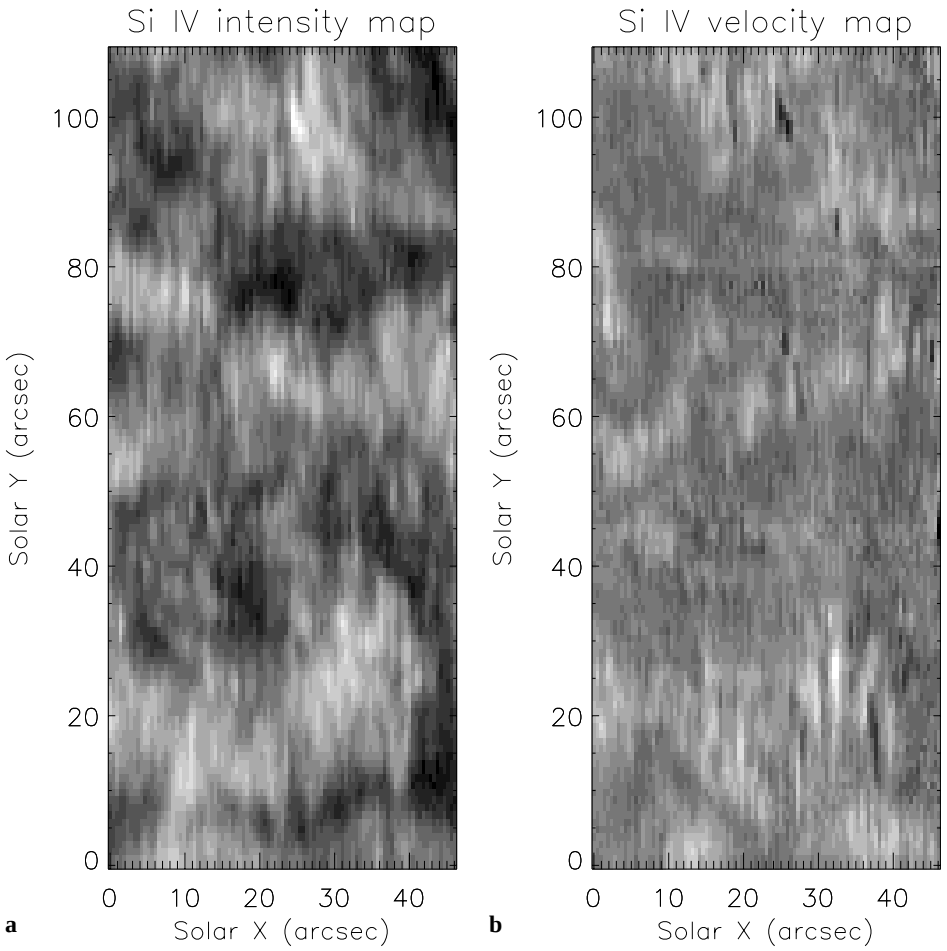

Fig. 1. a Si IV intensity maps (logarithmic scale) for the SEP17 quiet Sun raster at disk centre. **b** Si IV line shift map for the SEP17 quiet Sun raster; brighter pixels correspond to red-shifted positions.

line profiles were fitted to the strongest lines in all the spatial pixels of both datasets. Maps of intensity, spectral line position and width were created for each of the following lines: O V 629.8 Å, N V 1238.8 Å, Si IV 1402.8 Å.

The presence of a Si II line close to the O V line enabled the determination of the chromospheric network pattern in the SEP16 dataset; the second order Mg X line at 624.9 Å provided an intensity map at coronal temperatures. These two lines however are too weak to allow an accurate Gaussian fit, and their intensity maps have been determined simply by summing all the counts in a wavelength range centered on the peak wavelength and subtracting the background emission. In the case of Mg X the contribution of a blended, unidentified chromospheric line has been subtracted from the total intensity.

The resulting intensity maps have been deconvolved from the instrumental *point spread function* (Wilhelm et al. (1995) (PSF) using a maximum entropy algorithm part of the standard IDL^{TM} software, in order to improve spatial resolution on these maps.

The SEP17 intensity map (on a logarithmic scale) for Si IV is given in Fig. 1a. A portion of the field of view in the SEP16 intensity maps is presented in Fig. 2 (O V), Fig. 3a (Si II) and Fig. 3b (Mg X). The temperature of formation of O V is around T$\approx 10^{5.4}$ K; Si IV is formed at T$\approx 10^{4.8}$ K; Si II formation temperature is around 10^4 K; the Mg X ion peaks at Log T$\approx 10^{6.05}$ K.

The intensity maps of the two transition region lines displayed in Fig. 1a and Fig. 2 reveal the presence of a multitude of fine structures in the quiet Sun. These can be identified as filamentary patterns of brighter emitting material distributed across the whole field of view. These structures seem to be clustered together in large concentrations which constitute the whole of the brighter areas in Figs. 1a and 2. However, in many cases these brighter structures are extended also over the darker areas.

These filamentary structures seem to be overlying the chromospheric network, as seen through the intensity map of the Si II 1258.8 Å line in Fig. 3a; they account for $\approx$ 75% of the total intensity emitted in these lines in the whole field of view, and they are at the limit or below the instrumental spatial resolution. Fig. 1a and 2 seem to suggest that these structures are mostly composed by a large number of small transition region loops crossing the network boundaries and sometimes overlying supergranular cells. No obvious signatures of these transition region structures appear to be present in the Mg X intensity map, which, on the contrary, appears to be much smoother and less structured. However the Mg X emission does appear to be strongest where there is a cluster of Si II emission.

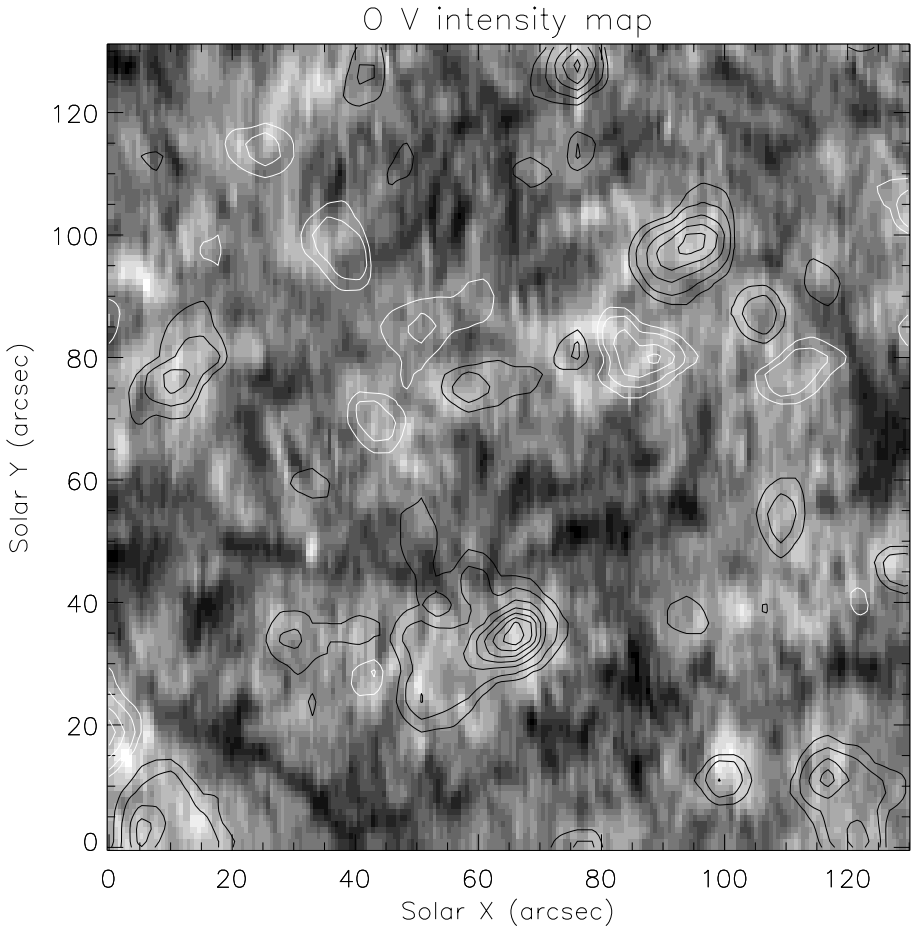

Fig. 2. O V intensity map (logarithmic scale) for the SEP16 quiet Sun raster near disk centre. Contour plots represent the photospheric magnetic field: white means positive polarity, black negative polarity.

Figs. 2 and 3 also display the contours of the photospheric magnetic field overplotted to the intensity maps. The magnetic field image has been taken from a full-disk magnetogram obtained by the Kitt Peak observatory, and has been co-aligned with the SUMER field of view. Unfortunately, the sensitivity and the spatial resolution of the magnetogram are too poor to help in determining the correlation (if there is any) between the SUMER fine structures observed in the O V emission and the photospheric magnetic field. It is possible to see that the magnetic field is stronger where the Si II emission is brightest and most of the filamentary structures are located, but no conclusion on possible relationship between individual structures and magnetic field can be drawn. However, it is possible to see that the some of the strongest magnetic field signatures are correlated with the larger coronal structures as seen in Mg X. In particular, the brightest Mg X emission in the field of view is correlated with areas containing enhanced magnetic field of opposite polarity.

A much higher spatial resolution and sensitivity of the magnetograph are required in order to be able to correlate individual transition region fine structures and the magnetic field.

Figs. 1b (Si IV) and 4 (O V) show maps of the fitted spectral line position for the two quiet Sun regions (SEP17 and SEP16). The bright pixels in the spectral line shift map correspond to red-shifted material. In both datasets, there is a correlation between the fine structures and the spectral line position. There is a trend of red-shifted emission along the bright filamentary structures relative to darker locations surrounding them. Given the small-scale nature of this trend, it is not easy to correlate these apparent motions with the photospheric magnetic field, also displayed in Fig. 4. From Fig. 4 it is only possible to see that the largest shifts seem to be correlated with stronger magnetic field, but the low spatial resolution of the Kitt Peak images prevents from drawing any further conclusion. On average, the relative motion between plasma in structures and plasma outside structures is ≈ 6 km s^{-1} for O V. More details of the analysis of the spectral line shifts are given in the next section.

The intensity maps for the transition region emission also show that there are a number of small active locations scattered all over the field of view. During the 60 seconds exposure time (Fig. 2), bright elements (explosive event locations) are seen preferentially along the slit (or y axis), while the solar rotation and the width of the slit limit the spatial extent along the x axis. These small active structures are located above the chromospheric network. At these locations, the line profiles are distorted from the Gaussian shape which is prevalent in the quiet Sun data. The line shape in these small active locations (explosive events) shows secondary peaks, possibly corresponding to turbulence or fast plasma motions along the line of sight. A larger-scale explosive event was also observed in the present

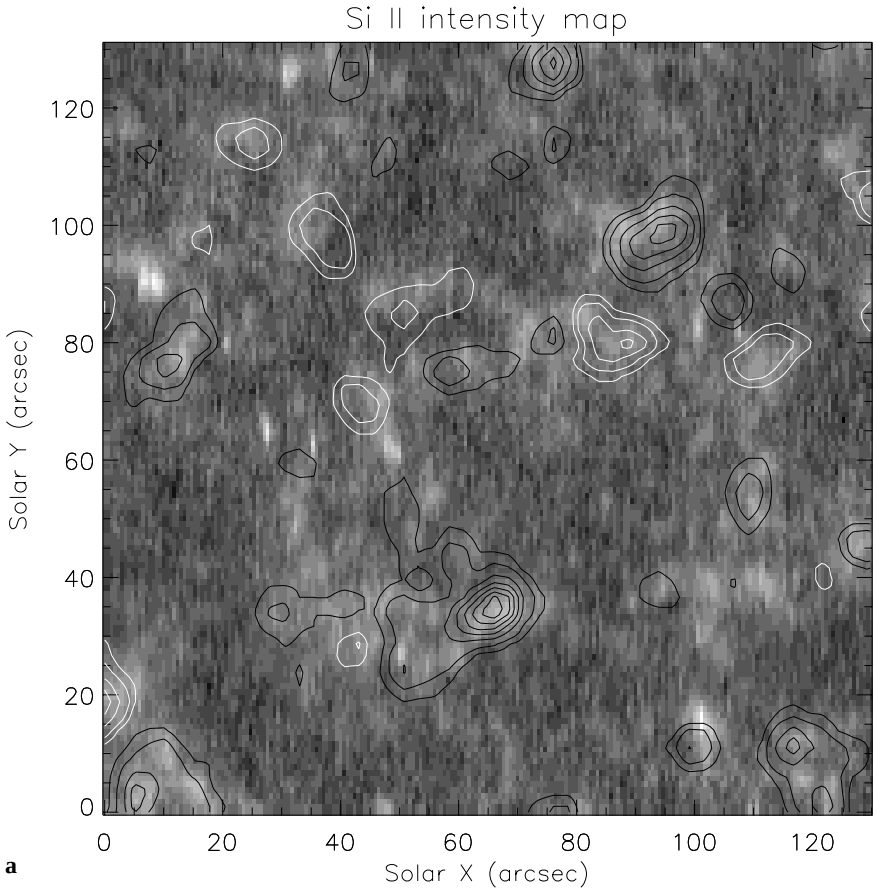

a

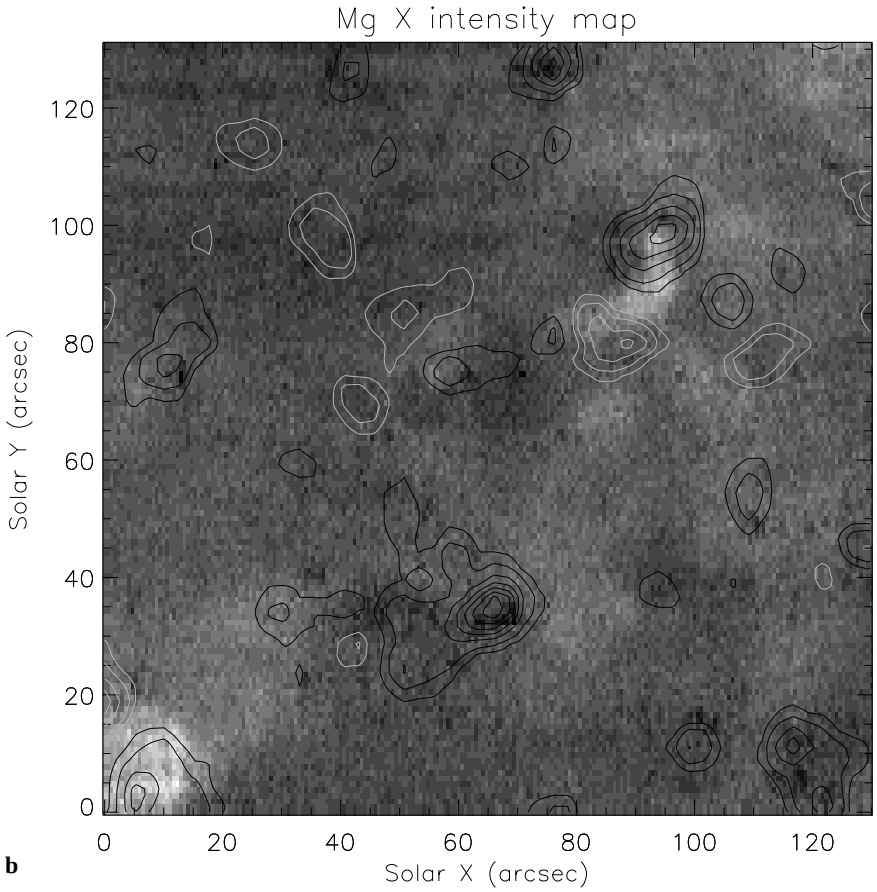

b

Fig. 3. Si II **a** and Mg X **b** intensity maps (logarithmic scale) for the SEP16 quiet Sun raster at disk centre. Contour plots represent the photospheric magnetic field: white means positive polarity, black negative polarity.

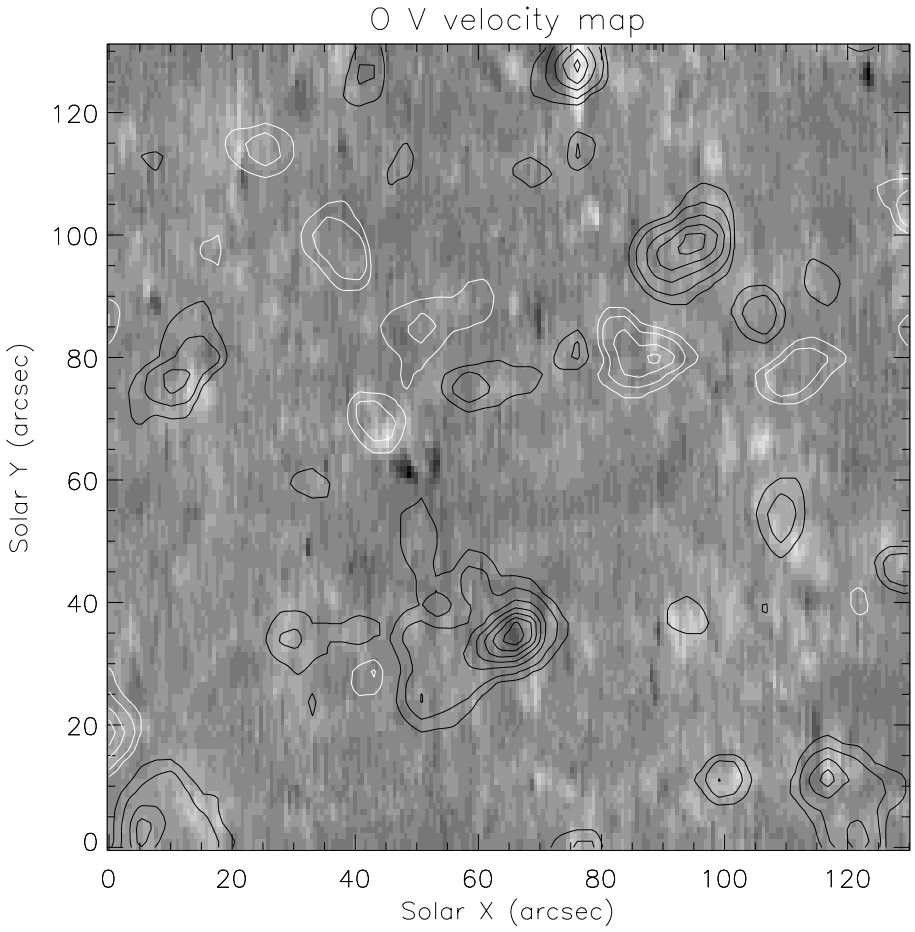

Fig. 4. Spectral line shift map for the O V line. Brighter pixels correspond to red-shifted positions. Contour plots represent the photospheric magnetic field: white means positive polarity, black negative polarity.

dataset (outside the field of view displayed in Fig. 2). This corresponds to a rather wide region where line profiles are very irregular, possibly a jet-like structure. These small active features, and the jet-like structure, will be discussed in detail in Sect. 5.

4. Diagnostics on the emitting region

Figs. 1, 2 and 4 indicate a relationship between relative redshifts and intensities for the transition region lines. They also show that the brighter pixels belong to the fine structures which appear to be loops of varying sizes. To investigate these results further, we have divided each dataset into several classes according to the line intensity.

First, the fitted line intensities of O V (for the SEP16 dataset) and Si IV (for the SEP17 dataset) have been divided into 11 intensity classes. The spatial pixels included in each of these intensity classes determine a spatial "mask" into the field of view. Then, the spectrum of each dataset has been averaged according to these masks. This has produced 11 average spectra from each dataset: spectral lines have been fitted using Gaussian functions. It should be noted that the two brightest intensity classes include pixels where line profiles were heavily distorted due to plasma activity: in these two classes the averaged line profiles depart from a Gaussian shape and therefore fitted line positions and intensity ratios are not precise. The two lowest intensity classes correspond to the darker plasma outside the structures, while the remaining classes include emission from structured plasma.

4.1. Line position trends

The measured line positions are displayed in Fig. 5 for O V 2×629.7 Å, N V 1238.8 Å and Si IV 1402.8 Å. In all cases line positions become more red-shifted as the intensity increases. The maximum relative motions between the bright fine structures and dark unstructured plasma is 4.0 km s^{-1} (N V) and 6.0 km s^{-1} (O V and Si IV). The O IV 1401.2 Å line, which is weaker than the other lines, shows a similar trend, with relative motions up to 7.7 km s^{-1}. These values are somewhat lower than those given by Teriaca et al. (1999a) for the quiet Sun, particularly for N V.

Unfortunately, the lack of reliable measurements of chromospheric line positions prevented the determination of an absolute wavelength scale, so that it is not possible to say whether the darker plasma outside the structures is moving outward or the structured plasma is red-shifted relatively to the rest position. Other observations with SUMER indicate that the latter is the most likely scenario.

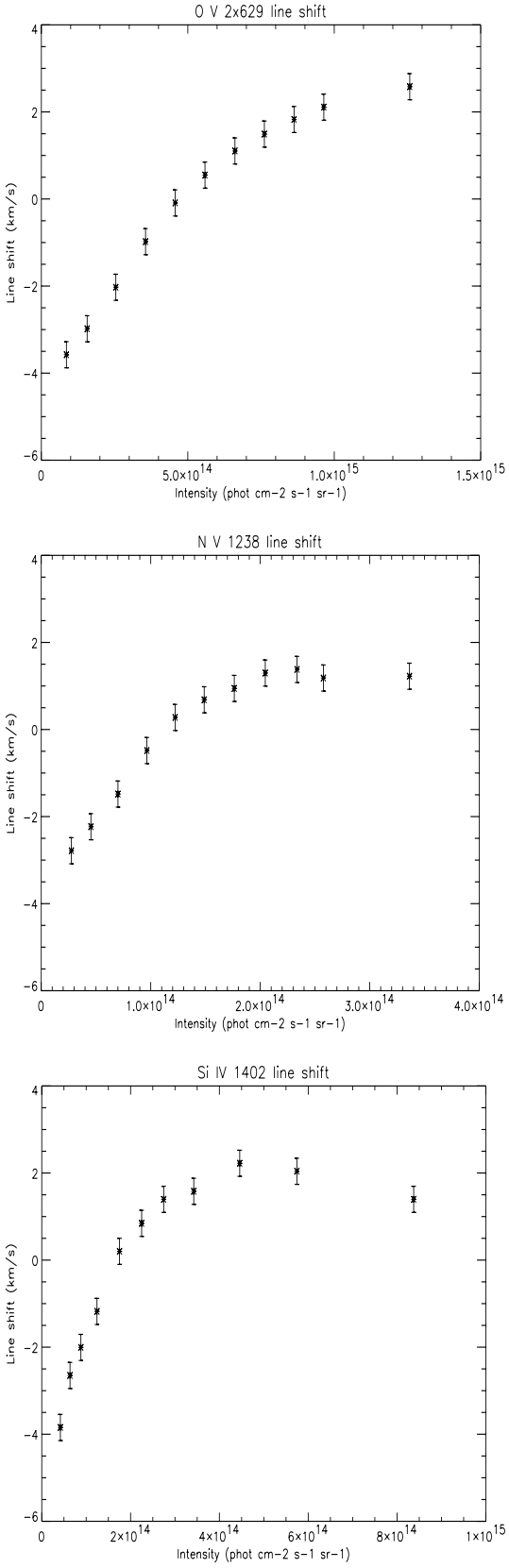

Fig. 5. O V 2×629.7 Å (*top*), N V 1238.8 Å (*middle*) and Si IV 1402.8 Å (*bottom*) fitted line position as a function of line intensity.

Table 2. Gradient of the ξ-I relation for Si IV, N V, O IV and O V observed lines.

Ion	Log T_{max}	Gradient
Si IV	4.80	$(1.38 \pm 0.05) \times 10^{-14}$
N V	5.24	$(1.86 \pm 0.09) \times 10^{-14}$
O IV	5.24	$(1.77 \pm 0.06) \times 10^{-12}$
O V	5.38	$(8.80 \pm 0.30) \times 10^{-15}$

4.2. Line width trends

Fitted line widths are displayed as a function of line intensity in Fig. 6 for Si IV 1402.8 Å, O V 2×629.7 Å and N V 1238.8 Å. Also the O IV 1401.2 Å line width has been measured. In all cases the spectral line width increases as intensity increases. It is to be noted however that the two highest intensity classes include active pixels where line profiles are severely distorted by plasma motions (see Sect. 5) and could not be reliably fitted with Gaussian functions: these pixels provide artificially high line widths and so the last two data points in Fig. 6 must be treated with caution.

Each intensity class includes a large number of pixels, whose fitted line positions are different from pixel to pixel due to relative small line shifts. When the emission of all pixels of each intensity class is averaged, these line shifts may introduce a spurious line broadening which needs to be removed. In order to correct for this, we have shifted the emission of each pixel along the wavelength direction to a fixed, arbitrarily chosen common value. The resulting spectrum has been averaged and fitted to obtain the corrected values for the line width. These are displayed in Fig. 6 as dashed lines. The resulting, corrected line widths are on the average smaller than the uncorrected values, but differences are quite small. It is important to note that the width versus intensity trend is confirmed.

4.3. Non-thermal speeds trends

The width-intensity relation has consequences on the non-thermal velocities in the emitting plasma. Signatures of a relation between line intensity and non-thermal velocities have been reported by Dere et al. (1984) for C IV and Dere & Mason (1993) for C IV and Si IV. They found that brighter regions show higher non-thermal velocities. More recently, Chae et al. (1998b) have measured non-thermal velocities for several ions spanning a temperature range from photosphere to the corona (C II, Si IV, C IV and O VI). These authors find the same trend, that lines formed at different temperatures show different degrees of correlation between line intensity and non-thermal speed.

In the present work, the use of the 'intensity classes' technique allows us to investigate this relation for Si IV, N V, O IV and O V. We determine the *most probable non thermal speed* ξ following the method described by Chae et al. (1998b). The resulting ξ vs. intensity curves are displayed in Fig. 7. It is possible to see a clear relation between the two quantities, although the gradient of the curve is different for different spectral lines. On average, ξ values determined in the present work are some-

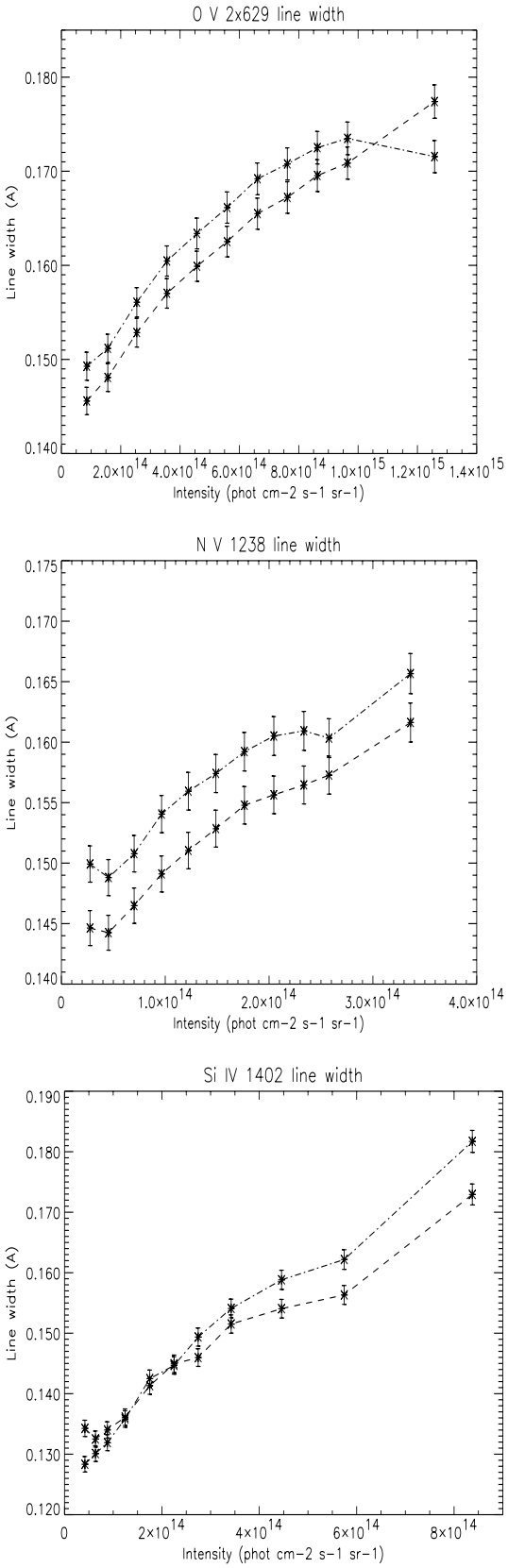

Fig. 6. O V 2×629.7 Å (*top*), N V 1238.8 Å (*middle*) and Si IV 1402.8 Å (*bottom*) fitted line width as a function of line intensity. The dash-dotted line indicates uncorrected line widths, the dashed line indicates the corrected line width (see text).

what higher than those reported by Chae et al. (1998b) and Dere & Mason (1993). In order to determine the gradient of the ξ-I relation we have rejected the two brightest measurements, as line profiles in these two intensity classes were corrupted by activity. We have fitted a linear curve on each of the plots and values for the gradients are reported in Table 2.

4.4. Electron density and temperature

The O IV spectral lines have frequently been used as a density diagnostic for the transition region plasma. It should be noted that with any density diagnostic techniques, only a rough 'average' density can be obtained, since the transition region is dynamic, highly structured and inhomogeneous.

O'Shea et al. (1998) investigated the 1401/1407 line ratio as a density diagnostic for the transition region, using SUMER data. However, the 1407.4 Å line is blended with the O III second order multiplet at 703.8 Å. Although it is possible to separate the O IV and O III lines, this leaves a greater uncertainty in the measured line intensities. Branching ratios with the isolated 1399.8 Å line show that the O IV 1407.4 Å line is stronger than expected. In this work, the 1401/1399 line ratio is preferred for density determination. These two lines are free from blending contributions but their ratio is slightly temperature dependent.

The electron density has been measured inside each averaged intensity class and results are displayed in Fig. 8 (top). Theoretical line ratios are taken from the CHIANTI database (Dere et al. 1997, Landi et al. 1999b). A consistent value of around 10^{10} cm^{-3} is found, with some trend to increase when the Si IV line intensity increases, although the uncertainties are quite large. The two lowest intensity classes provide only an upper limit to the electron density. An indication of a correlation between intensity and electron density has been reported by Griffiths et al. (1999). They found that electron density increases as intensity increases.

The line ratio O V 629.8 / N V 1238.8 is temperature dependent, but its value is sensitive to changes in the relative O/N abundance. This intensity ratio is density insensitive for $N_e < 10^{11}$ cm^{-3}. The ion fractions used to calculate the theoretical ratio come from Arnaud & Rothenflug (1985), and the relative O/N abundance is taken from Feldman (1992). Fig. 8 (bottom) gives the resulting values for the intensity ratio. It shows that the temperature is approximately constant with intensity, except for the lowest classes, corresponding to dark plasma outside the bright structures. The change in temperature is less than 10% even though the ratio has a strong temperature dependence. The measured electron temperature value is $(1.82 \pm 0.13) \times 10^5$ K; this value is very close to the O IV maximum abundance temperature in ionization equilibrium.

As O IV is formed at temperatures very similar to the value determined by the O V/N V ratio, we can determine the electron pressure P_e using the measured electron temperature and electron density values. We assume that the quiet Sun plasma observed in the two different dates has on the average the same characteristics. The resulting electron pressure is between 7.2×10^{14} and 3.6×10^{15} K cm^{-3}. This pressure range is about

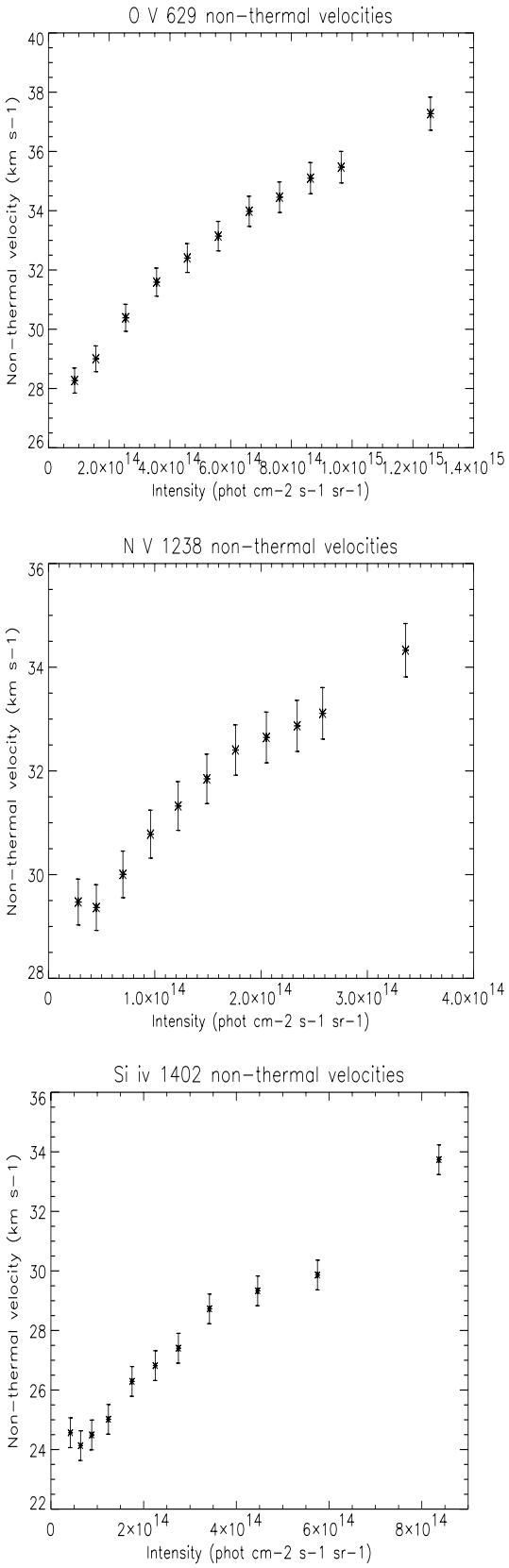

Fig. 7. O V 2×629.7 Å (*top*), N V 1238.8 Å (*middle*) and Si IV 1402.8 Å (*bottom*) most probable non-thermal speed ξ as a function of line intensity.

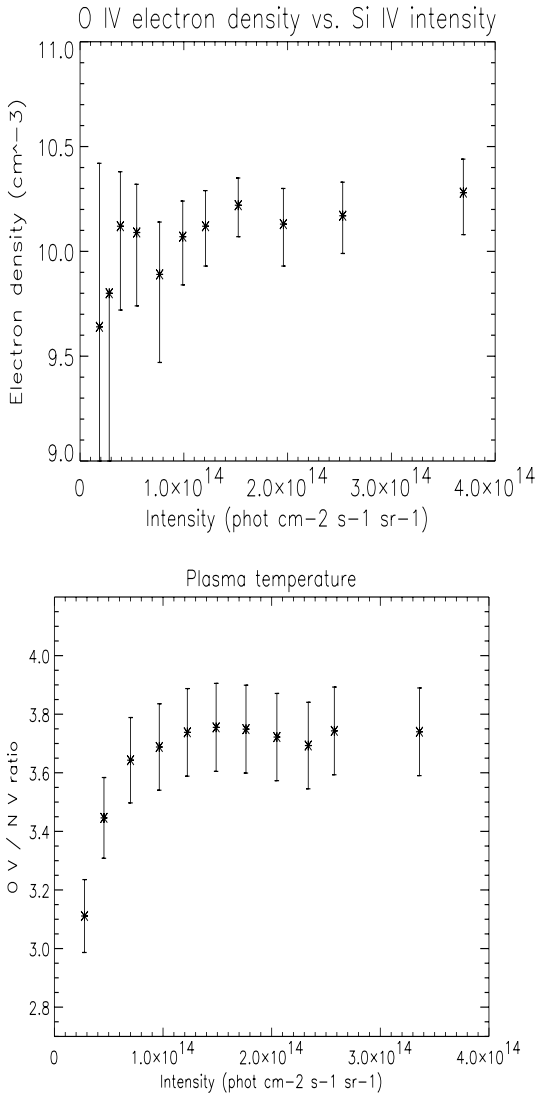

Fig. 8. *Top*: O IV electron density measurements from the SEP17 dataset as a function of Si IV 1402.8 Å line intensity. *Bottom*: O V/N V line ratio as a function of O V line intensity from the SEP16 dataset.

a factor ≈ 2 lower than the estimate by O'Shea et al. (1998) for active region conditions, and is in good agreement with the values obtained by Doscheck et al. (1998) and Griffiths et al. (1999) for several quiet Sun regions.

Using the derived electron density from O IV and temperature from the O V/N V ratio, it is possible to estimate a value for the 'filling factor' from the emission line intensities from the fine structures (we have not used the two lowest intensity classes, which have large errors). We assume that the transition region at 2×10^5 K is composed of isothermal loops with a 2 arcsec (1400 km) diameter. For N V, O V and Si IV, we find 'fill factors' which range from 5×10^{-3} to 5×10^{-2}, correlated with intensity. The values for these three lines are nearly identical. These values are similar to those derived by Dere et al. (1987). If we attempt to derive a 'fill factor' from the O IV lines, we obtain values which are two orders of magnitude smaller. This might suggest that the ionisation ratios for O IV are not at

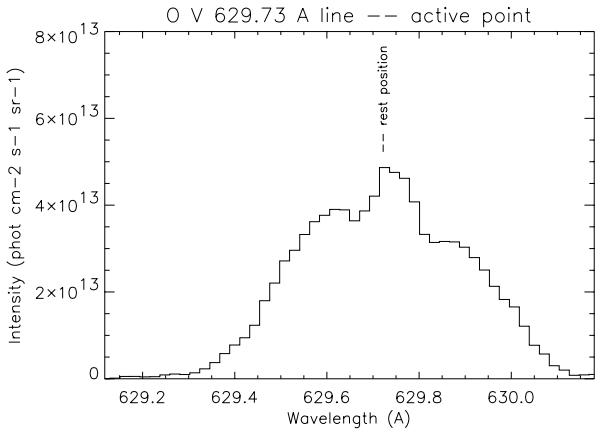

Fig. 9. O V 629.73 Å line profile in an active point.

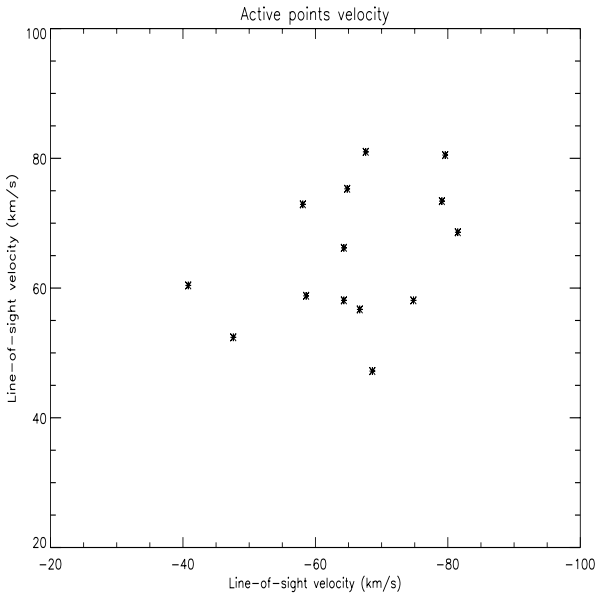

Fig. 10. Velocity shifts measured from the multi-Gaussian fits for some active points from Si IV and O V spectral line profiles. Abscissae: blue-shifted component; ordinate: red-shifted component.

the equilibrium values. However, further work is in progress on this important subject.

Since the electron density which we derived (Fig. 8, top) stays approximately constant, we surmise that the increase in intensity is due to a greater number of unresolved filaments within the loop-like structures for the brighter network locations.

5. Active features

5.1. Transition region explosive events

There are a large number of small explosive events, just a few pixels wide, in both quiet Sun datasets. They are located mostly over or close to the bright chromospheric network pattern. Often they do not show significantly enhanced intensities relative to the surrounding emission in quieter areas. These explosive events were detected by distortions in the spectral line profile, that is through the greater value of the single-Gaussian line width needed to fit the N V, O V and Si IV line profiles. The typical size of these explosive events is of the order of 2000 km. Given the duration of each single raster exposure, the lifetime of such events is between 1–4 minutes.

Line profiles in these small active locations are heavily distorted from the single-Gaussian line profile typical of the other surrounding quieter regions. An example of the spectral line profile can be seen in Fig. 9. It is possible to distinguish a central peak at approximately the rest wavelength, and two large wings, broadly symmetrical to the central unshifted line. The shape of the wings changes dramatically for different active points, and in some cases only *one* wing (generally the blue-shifted one) is visible in the spectrum.

The secondary blue and red-shifted peaks have been fitted for a sample of these explosive events assuming that both the central peak and the wings have Gaussian profiles. However, in many cases the wings of the profiles are very irregular and it is not easy to fit a single-Gaussian to them: in some cases *two* Gaussian profiles were necessary for the blue-shifted wing, and sometimes even then, the fit was poor. In contrast, an accurate single-Gaussian fit was always possible for the central, unshifted feature, and the resulting line position and width for the central part of the active point line profiles is very similar to the values obtained in the surrounding quieter plasma. This quiescent, central spectral feature could be due to quieter plasma along the line of sight.

The resulting spectral line positions and line-of-sight velocities relative to the average quiet Sun value are displayed in Fig. 10 for a sample of active points. The x-axis values represent the blueshifted line component and the y-axis values represent the corresponding red-shifted line component. From these data, it is possible to see that both red-shifted and blueshifted line-of-sight velocity lie in the 50–80 km s^{-1} range, with very similar values. The total intensity associated with the two line wings in each active point is different, the blue-shifted wing being more intense in nearly all cases. It is also worth noting that in some active points (not included in Fig. 10) only the blueshifted line component was observed.

Unfortunately, the heavy distortion of the line profiles for these explosive events did not allow a reliable fit for the density-dependent O IV lines, so that estimates of electron densities were not possible. The behaviour of these explosive events is the same for all the transition region lines: Si IV, O V and N V. This suggests that the structures generating this activity are coherent over the different temperatures of formation of these lines. In contrast, no correlation has been found between the Mg X spectral line behaviour and the transition region activity, indicating that this activity is confined to transition region temperatures.

These kind of events are not new in solar observations. They were first observed by Brueckner & Bartoe (1983), which called them *turbulent events*. Later analyses showed that turbulence was not the cause of these phenomena and they were referred to as *explosive events*. Dere et al. (1989) report the physical characteristics of a large number of explosive events, which are broadly consistent with those described in the present study.

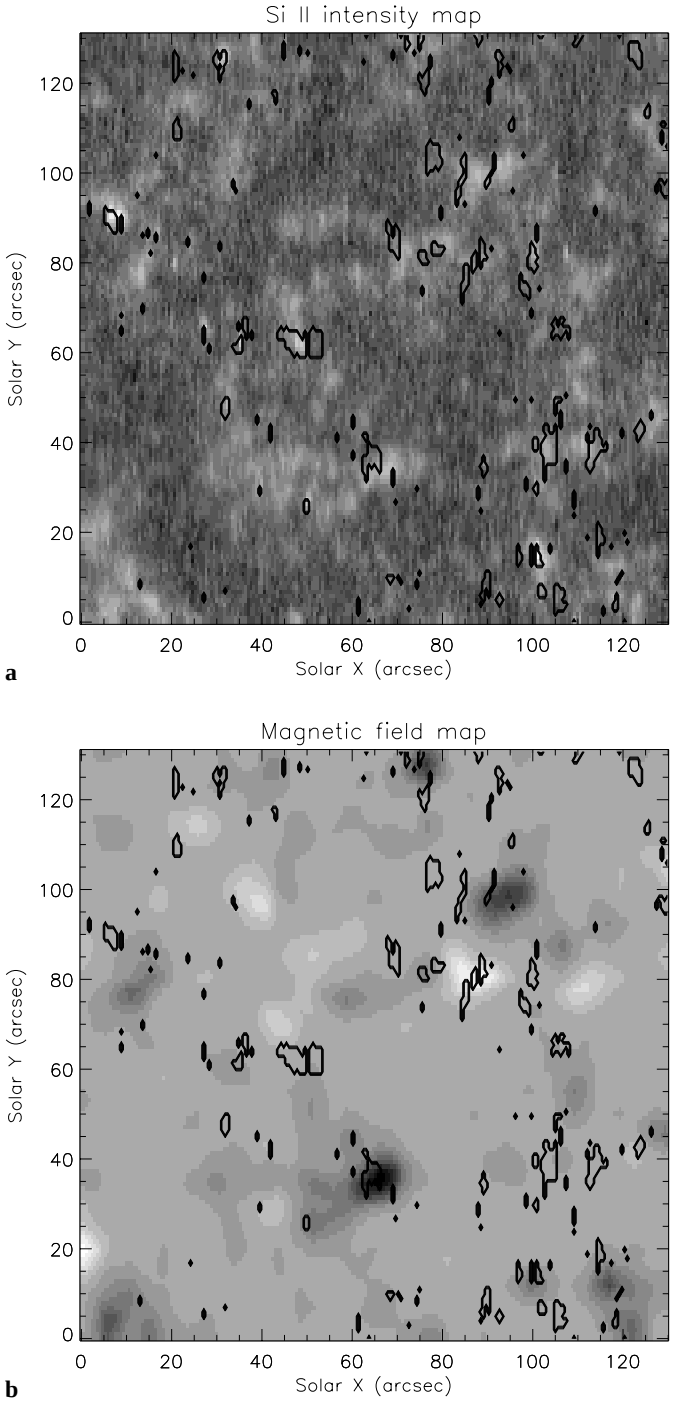

Fig. 11. a Si II intensity map with the locations of active points superimposed. **b** Kitt Peak magnetogram with the locations of active points superimposed. Active point areas are circled by black lines on the intensity maps. Black means negative polarity, white positive polarity.

Fig. 11a shows the locations of the active points relative to the cell-network structure, as defined by the Si II intensity map. The active events take place either over the network pattern or in the region very close to it. The occurrence frequency of such activity falls dramatically in the cell interiors. Some clusters of active points are found where the Si II emission is strongest, but isolated points are found mostly at the edges of Si II bright network. Fig. 11b attempts to correlate the bright points with the photospheric magnetic field from the Kitt Peak images. It is possible to see from Fig. 11b that the largest number of the active points is not correlated with the stronger photospheric magnetic field but is located outside of the magnetic features. Unfortunately, the sensitivity and spatial resolution of the magnetogram does not allow to detect the presence of possible weaker magnetic field features correlated with the active points. It is interesting to see that in the cases where bright points and magnetic field are correlated, the bright point is sitting on top of magnetic field of the same polarity.

In the past, a few attempts have been made to correlate magnetic field and explosive events, mainly by Dere et al. (1991) and Porter & Dere (1991). They found that most explosive events are not correlated with the strongest features of the magnetic field, but are found at the boundaries of the network. Only in a few cases are transition region explosive events correlated with X-ray bright points, magnetic bipoles or a neutral line of an emerging active region.

5.2. A jet-like structure

In the SEP16 dataset a large active area was observed at (40″, 95″) in the field of view displayed in Fig. 2: this region can be seen as the brightest area in the whole intensity map in both N V and O V lines. This active area is ≈ 3500 km long along the slit length, and around 7000 km wide in the solar X direction. From the time which the SUMER slit took to cover the observed extent of this structure (rastering toward the east limb), we can deduce that the lifetime of the activity is at least 10 minutes.

The most striking feature of this dynamic feature is a huge jet-like structure which seems to be rooted in the core of the active area and extends toward the south, slightly inclined relatively to the SUMER slit. The spectral line profile is extremely distorted, showing a large, non-Gaussian blue-shifted component superimposed on a regular profile similar to the quiet areas. Fig. 12 shows an image of this structure. The image represents an intensity map obtained by summing all the counts under the O V blue-shifted line profile, from 0 to -300 km s^{-1}. The feature seems to comprise two loop-like, or jet-like plasmas moving very fast and originating from the same central active area. The longest feature is around 14000 km long, and is inclined at around 10^o relative to the N-S direction. Unfortunately, it is not possible to distinguish between a loop, with very dynamic plasma flowing along its length, and a plasma jet. The N V line profile shows a very similar behaviour, although the longest of the two jet-like structures in Fig. 12 appears to be slightly shorter than the O V counterpart.

Assuming that this feature is a jet, the slight inclination relative to the SUMER slit allows the measurement of the velocity perpendicular to the line of sight. Also assuming that the bright emission in Fig. 12 at different slit positions comes from the same plasma which has moved eastward, we have estimated the speed perpendicular to the line of sight as being between 60 and 100 km s^{-1}. Combining this velocity with the estimate of

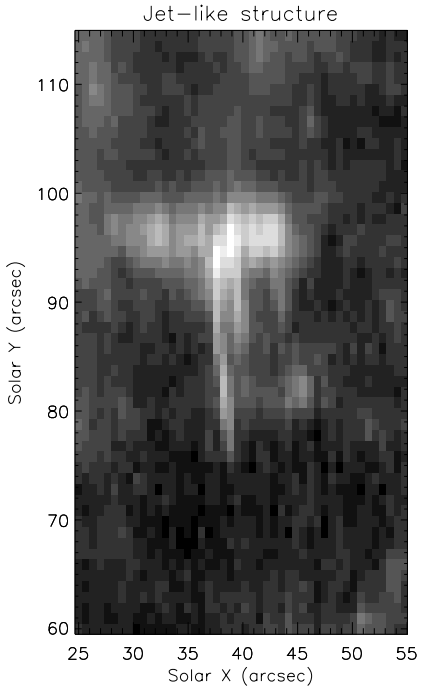

Fig. 12. The jet-like structure observed in the SEP16 dataset.

the line-of-sight velocity obtained from the line profile, gives a rough estimate of the plasma absolute speed as between 180 and 270 km s^{-1}. The uncertainty of the measured speed is large due to the breadth of the extended blue-shifted component. It is interesting to note that no signature of a red-shifted counterpart of the observed feature is observed anywhere in the active area.

6. Discussion and conclusions

6.1. Quiet Sun

Our observations and analysis indicate that most of the emission from transition region temperatures ($\approx 2 \times 10^5$ K) comes from fine structures, which appear to be low lying loops across the network boundaries. This is consistent with the type of model proposed by Feldman (1983) and Dowdy et al. (1986). Feldman et al. (1999) published large images produced by SUMER in the C III (977 Å) and S VI (933 Å) spectral lines corresponding to temperatures of around 8×10^4 K and 2×10^5 K respectively. They observed low lying loop structures in C III emission apparently randomly and sparsely distributed in the cell centre, but intense and clumped across the network boundaries. The signal to noise was not as good for the S VI emission, so the fine structures were not so obvious. Our results confirm their conclusions on the morphological nature of the quiet solar transition region. We have extended their work with better observations at 2×10^5 K and we provide a detailed, quantitative investigation into some of the physical properties (electron density and temperature, filling factor, plasma motions) of these unresolved fine structures. We are not able to draw any conclusions about whether or not the coronal emission is also confined in loop structures, since the Mg X emission which we observe is too weak. Other observations, from TRACE, suggest that the coronal emission from the quiet Sun is also predominantly in loop structures. It is difficult to conceive how transition region models based on the idea of a transition region as a thin, continuous interface between the photosphere and the corona could reproduce these observations.

There are a few different models in the literature which attempt to explain the down-flows seen at transition region temperatures. Hansteen (1993) and Hansteen et al. (1996) considered nano-flares occuring at the top of coronal loops. Following the suggestion of Peter & Judge (1999), the numerical model by Teriaca et al. (1999b, 1999c) extends these ideas and proposes that the pattern of Doppler shift as a function of temperature can be explained by the occurence of nano-flares in magnetic loops at a temperature of around 3×10^5 K. This new insight into transition region dynamics explains the net redshifts of 11 km s^{-1} found for lines in the quiet solar atmosphere formed at around 1.5×10^5 K. Their simulations predict intensities for C IV, O VI and Ne VIII lines. There is a tendancy for the higher intensities for the C IV spectral line to be more redshifted. In order to reproduce our observations, the nano-flare process would need to be continuously taking place in the cool transition region loops. We note that this model predicts that the plasma is not in ionisation equilibrium. It would be interesting to know if such numerical models can reproduce the specific behaviour of line-shift versus intensity which we have determined.

Teriaca et al. (1999d) claim that their model is also able to explain the distribution of non-thermal velocities as a function of temperature. Indeed, they propose that the larger range of values detected for active regions could be explained in terms of a higher frequency of occurrence and/or energy deposition of nano-flares in the middle-high transition region. Again it would be interesting to learn if such models could predict the strong correlation which we have found between intensity and non-thermal velocities.

Fig. 8 (top) shows that the electron density does not change markedly between darker plasma and structure. Intepreting darker regions as cell plasma and bright regions as structured network plasma, means that the electron density values at transition region temperatures are similar in the network and cells. A similar behaviour has been recently noted by Del Zanna & Bromage (1999) in coronal hole and quiet Sun observations obtained by the Coronal Diagnostic Spectrometer on SOHO using O IV lines. Earlier measurements by Dupree et al. (1976) using C III lines observed by Skylab show a similar trend. Our measurements disagree with those by Vernazza & Reeves (1978), who report higher densities in network areas relative to cell centres as obtained from C III lines. Our results suggest that the differences in intensities observed between cell centres (dark areas) and network (bright structured plasma) are mainly due to differences in filling factors in these different areas.

6.2. Dynamic activity

A comprehensive review of the characteristics of explosive events from HRTS observations of C IV was provided by Dere

et al. (1989) and Dere (1994). It is of interest to compare our results with theirs. The size, maximum velocities and lifetimes we obtain are comparable. The profiles are also usually asymmetric. Dere (1994) suggests that the explosive events are caused by magnetic reconnection near the edges of strong network field regions. He said that 'the basic picture is that small magnetic bipoles emerge in the supergranular cell centres and are transported to the boundaries where opposite polarity flux elements are driven together by photospheric flows and forced to cancel'. This type of scenario does indeed seems to have been confirmed by more recent SOHO observations. Dere found that the explosive events appear to occur low down, just above the photosphere.

The numerical model by Sarro et al. (1999), Erdelyi & Sarro (1999) allows for an energy release to take place in a semicircular flux tube, at a height just below the transition region. This generates upwards and downwards flows along the loop as well as a rise in temperature and sound waves which develop into shocks. As a result, new transition regions moving at opposite velocities are created. The signature of these flows can be associated with distorted line profiles with red and blue components. If there is an ensemble of filamentary quiescent loops present, with just one loop undergoing an energy injection, then a central profile with perturbed wings would be observed, consistent with observations.

A sophisticated numerical model of explosive events in a 2D environment is presented by Roussev et al. (1999). Preliminary results are encouraging, but detailed spectroscopic predictions are still required. Innes & Toth (1999) present a model for explosive events, based on compressible MHD simulations of the evolution of a current sheet to a steady Petschek, jet-like configuration. They are able to reproduce the broad line profiles with extended wings in the temperature range 8×10^4 K to 2×10^5 K. They also explain how jets flowing outward into the corona are more extended and appear before jets flowing towards the chromosphere.

These numerical models, combined with a comprehensive analysis of observational evidence, provide a real opportunity for understanding the nature of the transition region fine structures.

Acknowledgements. We wish to thank U. Schühle, K. Wilhelm, K. Bocchialini and Espen Sollum for useful discussions and comments. We wish to thank also the referee, Dr. K.P.Dere, for his very helpful comments on the submitted manuscript. The SUMER project is financially supported by DLR, CNES, NASA and ESA PRODEX programme (Swiss contribution). SOHO is a mission of international cooperation between ESA and NASA. HEM acknowledges the financial support of PPARC. NSO/Kitt Peak data used here are produced cooperatively by NSF/NOAO, NASA/GSFC, and NOAA/SEL.

References

Antiochos S.K., Noci G., 1986, ApJ, 301, 440
Arnaud M., Rothenflug R., 1985, A&AS 60, 425
Benz A.O., Krucker S., 1999, A&A 341, 286
Berghmans D., Clette F., Moses D., 1998, A&A 336, 1039
Brekke P., Hassler D.M., Wilhelm K., 1997, Sol. Phys. 175, 349
Brynildsen N., Brekke P., Fredvik T., et al., 1998, Sol. Phys. 181, 23
Brueckner G.E., Bartoe J-D.F., 1983, ApJ 272, 329
Chae J., Wang H., Lee C., Goode P.R., Schühle U., 1998a, ApJ 497, L109
Chae J., Schühle U., Lemaire P., 1998b, ApJ 505, 957
Del Zanna G., Bromage B.J.I., 1999, J. Geoph. Res. 104, 9753
Dere K.P., Bartoe J.-D. F., Brueckner G.E., 1984, ApJ 281, 870
Dere, K.P., Bartoe J.-D. F., Brueckner G.E., Cook J.W., Socker D.G., 1987, Sol. Phys. 114, 223
Dere K.P., Bartoe J.-D.F., Brueckner G.E., 1989, Sol. Phys. 123, 41
Dere K.P., Bartoe J.-D.F., Brueckner G.E., Ewing J., Lund P., 1991, J. Geoph. Res. 96, 9399
Dere K.P., Mason H.E., 1993, Sol. Phys. 144, 217
Dere K.P., 1994, Adv. Space Res. 14, (4) 13
Dere K.P., Landi E., Mason H.E., Monsignori Fossi B.C., Young P.R., 1997, A&AS 125, 149
Doyle J.G., O'Shea E., Erdelyi R., et al., 1997, Sol. Phys. 173, 243
Doscheck G.A., Feldman U., Laming J.M., et al., 1998, ApJ 507, 991
Dowdy J.F. Jr., Rabin D., Moore R.L., 1986, Sol. Phys. 105, 35
Dupree A.K., Foukal P.V., Jordan C., 1976, ApJ 209, 621
Erdelyi R., Doyle J.G., Perez M.E., Wilhelm K., 1998a, A&A 337, 287
Erdelyi R., Sarro L.M., 1999, In: Kaldeich B. (ed.) Proc. of the 8th SOHO Workshop, Plasma Dynamics and Diagnostics in the Solar Transition region., ESA-SP 446, in press
Feldman U., 1983, ApJ 275, 367
Feldman U., 1992, Phys. Scripta 46, 202
Feldman U., Laming J.M., 1994, ApJ 434, 370
Feldman U., Widing K.G., Warren H.P., 1999, ApJ 522, 1133; 2000, ApJ 529, 1145
Gabriel A.H., 1976, Phil. Trans. R. Soc. London, Ser. A 281, 339
Gabriel A.H., Mason H.E., 1982, In: Applied atomic collision physics. Vol. 1, Academic Press, New York, London, p. 345
Gallagher P.T., Phillips K.J.H., Harra-Murnion L.K., Baudin F., Keenan F.P., 1999, A&A 348, 251
Griffiths, N.W., Fisher G.H., Woods D.T., Siegmund O.H.W., 1999, ApJ 512, 992
Hansteen V.H., 1993, ApJ 402, 741
Hansteen V.H., Maltby P., Magagoli A., 1996, In: Bentley R.D., Mariska J.T. (eds.) Magnetic Reconnection in the Solar Atmosphere. ASP Conf. Ser. 111, p. 116
Harrison R.A., Sawyer E.C., Carter M.K., et al., 1995, Sol. Phys. 162, 233
Harrison R.A., 1997, Sol. Phys. 175, 467
Harrison R.A., Lang J., Brooks D.H., Innes D.E., 1999, A&A in press
Innes D.E., Brekke P., Germerott D., Wilhelm K., 1997, Sol. Phys. 175, 341
Innes D.E., Toth G., 1999, Sol. Phys. 185, 127
Krucker S., Benz A.O., 1998, ApJ 501, L213
Landi E., Mason H.E., Landini M., 1999a, Space Sci. Rev. 87, 241
Landi E., Landini M., Dere K.P., Young P.R., Mason H.E., 1999b, A&AS 135, 339
Lemaire P., Wilhelm K., Curdt W., et al., 1997, Solar Phys. 170, 105
O'Shea E., Doyle J.G., Keenan F.P., 1998, A&A 338,1102
Parker E.N., 1998, Adv. Space Res. 21, 267
Peter H., 1999, ApJ 516, 490
Peter H., Judge P.G., 1999, ApJ 522, 1148
Porter J.G., Dere K.P., 1991, ApJ 370, 775
Roussev I., Erdelyi R., Doyle J.G., Galsgaard K., 1999, Sol. Phys. in press

Sarro L.M., Erdelyi R., Doyle J.G., Perez E.P., 1999, A&A 351, 721
Teriaca L., Banerjee D., Doyle J.G., 1999a, A&A 349, 636
Teriaca L., Doyle J.G., Erdelyi R., Sarro L.M. 1999b, A&A 352, L99
Teriaca L., Doyle J.G., Erdelyi R., Sarro L.M., Banerjee, D., 1999c, In: Wilson A. (ed.) Proc. of the 9th European Meeting on Solar Physics, Magnetic Fields and Solar Processes. ESA-SP 448, in press
Teriaca L., Banerjee D., Doyle J.G., Erdelyi R., 1999d, In: Kaldeich B. (ed.) Proc. of the 8th SOHO Workshop, Plasma Dynamics and Diagnostics in the Solar Transition region. ESA-SP 446, in press
Vernazza J.E., Reeves E.M., 1978, ApJS 37, 485
Wilhelm K., Curdt W., Marsch E., et al., 1995, Solar Phys. 162, 189
Wilhelm K., Lemaire P., Curdt W., et al., 1997, Solar Phys. 170, 75
Wikstol O., Judge P.G., Hansteen V., 1998, ApJ 496, 117